TB, TD, US, PMB/252053, 30/01/2008

IOP PUBLISHING PHYSICS IN MEDICINE AND BIOLOGY

Phys. Med. Biol. **53** (2008) 1–15 UNCORRECTED PROOF

In vitro characterization of the subharmonic ultrasound signal from Definity microbubbles at high frequencies

K Cheung[1], O Couture, P D Bevan, E Cherin, R Williams, P N Burns and F S Foster[2]

Imaging Research, Sunnybrook Health Sciences Centre/University of Toronto, Toronto, Canada

E-mail: kcheung@swri.ca and stuart@swri.ca

Received 4 June 2007, in final form 7 January 2008
Published DD MMM 2008
Online at stacks.iop.org/PMB/53/1

Abstract

Ultrasound microbubble contrast agents have been demonstrated to scatter subharmonic energy at one-half the driving frequency. At ultrasound frequencies in the 20–40 MHz range, the subharmonic offers the potential to differentiate the blood in the microcirculation from the surrounding tissue. It is unknown whether current contrast agents, manufactured to be resonant between 2 and 12 MHz, are ideal for subharmonic imaging at higher frequencies. We performed numerical simulations of the Keller–Miksis model for the behavior of a single bubble and experimental investigations of Definity microbubbles in water. The results supported the hypothesis that off-resonant bubbles, excited at their second harmonic, may be primarily responsible for the observed subharmonic energy. For frequencies between 20 and 32 MHz and 32 and 40 MHz, the optimal bubble diameters for the generation of subharmonics *in vitro* were determined experimentally to be 1.2–5 μm and less than 1.2 μm, respectively. Definity may be a suitable ultrasound contrast agent for subharmonic imaging at 20 MHz with peak-negative pressures between 380 and 590 kPa and pulses greater than or equal to four cycles in duration.

1. Introduction

The formation of blood vessels, through a process known as angiogenesis, is fundamental to the proliferation of healthy tissue and disease processes such as cancer. The ability to non-invasively image blood flow in the microcirculation, consequently, may play an important

[1] Address for correspondence: Undergraduate Medical Education, Class of 2009, 68 Barrie Street, Kingston, ON K7L 3N6, Canada.
[2] Reprint requests should be addressed to Stuart Foster, Imaging Research, Sunnybrook Health Sciences Centre, 2075 Bayview Avenue, 6th Floor, S wing, Toronto, ON M4N 3M5, Canada.

role in the detection of early disease (Foster *et al* 2000a) and the evaluation of anti-angiogenic drugs (Kerbel 2001).

Ultrasound contrast agents, comprising gas bubbles less than 5 μm in diameter and encapsulated by a polymer or lipid shell, are an effective strategy for detecting and visualizing blood flow. These microbubbles are true intravascular agents and are used clinically to image the myocardium (Becher and Burns 2000). When placed in an ultrasound field, the microbubbles exhibit resonance due to the compressible nature of the gas inside the bubble. With increased incident amplitudes, the bubbles can be driven to oscillate asymmetrically resulting in the scattering of energy to harmonic multiples of the transmit frequency (f_o). Techniques such as harmonic imaging (Burns 1996) and pulse inversion (Simpson *et al* 1999) exploit the second harmonic ($2f_o$) to provide a greater contrast with respect to the surrounding tissue. The scattering of energy to subharmonic ($0.5f_o$) and ultraharmonic ($1.5f_o$, $2.5f_o$, etc) frequencies has also been observed (Shankar *et al* 1999, Forsberg *et al* 2000, Dayton and Ferrara 2002, Shi *et al* 2002).

The use of contrast agents at clinical frequencies (2–12 MHz), however, is poor at imaging the microcirculation due to limits in spatial resolution. High frequency ultrasound in the range of 20–40 MHz offers improvements in spatial resolution and, in conjunction with microbubble contrast agents, has been demonstrated to detect blood flow in the microcirculation (Goertz 2002). The advantages, limitations and implementation of high frequency ultrasound imaging have been described previously (Foster *et al* 2000b).

There are a number of challenges facing the use of contrast agents in high frequency ultrasound due to the frequency dependence of blood, tissue and microbubbles (Lockwood *et al* 1991, Shung and Thieme 1993). At high frequencies, blood can have an echogenicity similar to that of the surrounding tissue, while the enhancement due to microbubbles is decreased relative to the tissue. Second harmonic imaging techniques have not shown as dramatic an improvement due to increased tissue harmonics as a result of nonlinear propagation. Subharmonic imaging may be a better solution, as the subharmonic is unique to microbubbles and uncompromised by nonlinear propagation. This offers the potential to suppress the signal from the surrounding tissue below the noise floor. Preliminary *in vivo* implementations of subharmonic imaging in mouse and rabbit models have demonstrated the feasibility of this technique (Goertz *et al* 2005).

To further optimize subharmonic imaging at high frequencies, a better understanding of the nature and behavior of the observed subharmonic signal is required. Current ultrasound contrast agents are designed such that the majority of bubbles present in the population are resonant at clinical frequencies. By increasing the operating frequency to 20 MHz and higher, the number of bubbles excited at resonance account for a small volume fraction of the population. It is unknown whether current clinical contrast agents are ideal for generating subharmonic signals at high frequencies (Goertz *et al* 2003).

The subharmonic has been well characterized at clinical frequencies (Shi *et al* 1997, Krishna *et al* 1999, Chomas *et al* 2002, de Jong *et al* 2002). Unlike integer-ordered harmonics that continuously increase with the square of incident pressure (Leighton 1994, Chang *et al* 1995), subharmonics are dependent on a pressure threshold. This threshold is bandwidth dependent and at a minimum for bubbles excited at twice their resonant frequency (Eller and Flynn 1969, Plesset and Prosperetti 1977, Shi *et al* 1999). Exceeding this threshold, the subharmonic signal grows in strength with increasing pressure amplitude until a point of saturation is reached (Forsberg *et al* 2000). The threshold for generation of subharmonics has been determined experimentally at clinical frequencies for a number of different microbubble contrast agents (Shankar *et al* 1999, Shi *et al* 1999, 2002). It is unknown whether these characteristics continue to apply for operating frequencies in the 20–40 MHz range.

The physical origin of the observed subharmonic energy from microbubbles is poorly understood though four possible explanations have been suggested for free bubbles (Leighton 1994, Phelps and Leighton 1997): (1) transient cavitation, (2) subharmonic oscillation of bubbles excited at resonance, (3) resonant oscillations of bubbles excited at their second harmonic and (4) non-radial modes of oscillation. Transient cavitation can result in the release of harmonic and subharmonic energies as well as broadband acoustic emissions (Neppiras 1980), though the incoherent nature of this process may limit *in vivo* application. Bubbles excited at their resonant frequency undergo large radial oscillation, but as the subharmonic threshold is exceeded, it is predicted that this oscillation will undergo a bifurcation causing the radius to reach two different maxima during expansion. This alternating radial expansion at half the driving frequency results in subharmonic energy. A larger bubble, excited at its second harmonic, can also undergo a bifurcation that results in the double maxima observed for resonant bubbles. For these bubbles, the subharmonic pressure threshold is predicted to be at a minimum, and the scattered energy can be greater than that of resonant bubbles because of its larger size. Non-radial modes of oscillation, or surface waves, may scatter energy with a 'subharmonic' component if the geometric cross-section of the bubble, as seen by the transducer, changes at half the driving frequency. While surface waves have been observed (Goertz *et al* 2004), it has not been determined if they result in significant acoustic emissions.

In this paper, we hypothesize that the primary source of the observed coherent subharmonic signal arises from bubbles excited at their second harmonic and oscillating at their resonant frequency. To test this hypothesis, numerical simulations for the behavior of a single bubble in an ultrasound field are first performed to guide experiments. Experiments were performed in which the bubble population's size distribution was varied and the ultrasound transmit frequency, pressure amplitude and pulse bandwidth were adjusted. The bubbles were also tested to ensure that disruption was not significant and that the observed subharmonic signal was the result of coherent scattering.

2. Methods

2.1. Numerical simulations of single shelled bubbles in water

For the 20 MHz driving frequency, the two bubble sizes of interest are those excited at their resonant frequency and those, with a resonant frequency of 10 MHz, excited at their second harmonic. The sizes of these bubbles were predicted with Minnaert's equation, modified to include the bulk modulus of an encapsulating shell (Hoff 2001), as illustrated below:

$$f_o = \frac{1}{2\pi a_e}\sqrt{\frac{3\kappa p_o + 12G_s\frac{d_S}{a_e}}{\rho_L}}, \tag{1}$$

where f_o is the resonant frequency, a_e is the equilibrium bubble radius, κ is the polytropic exponent of the gas, p_o is the atmospheric pressure, G_s and the d_S are the shear modulus and thickness of the shell, respectively, and ρ_L is the density of the surrounding liquid.

The contribution of the bubble size, encapsulating shell, driving frequency, pressure amplitude and pulse bandwidth to nonlinear scattering was investigated using the Keller–Miksis model implemented in Matlab (v7, Mathworks, Natick, MA, USA) by Hoff (2001). This model assumes spherical oscillations of a single bubble in an infinite medium of water and extends the Rayleigh–Plesset model by considering a compressible medium with a constant speed of sound, independent of pressure. Since sound can propagate in this medium, this results in the natural inclusion of damping due to sound radiation. As such, the model is

better suited for considering excitation pulses of greater amplitude and higher frequency. The Keller–Miksis model is described by the equation

$$\ddot{a}a\left(1-\frac{\dot{a}}{c}\right)+\frac{3}{2}\dot{a}^2\left(1-\frac{1}{3}\frac{\dot{a}}{c}\right)-\left(1+\frac{\dot{a}}{c}\right)\left(\frac{p_L-p_o-p_i\,(t+a/c)}{\rho}\right)-\frac{a}{\rho c}\dot{p}_L=0, \qquad (2)$$

where p_i is the incident pressure, p_o is the equilibrium pressure, p_L is the pressure at the surface of the bubble, ρ is the density of the liquid, a is the bubble's radius with respect to time, and $\dot{a}$ and $\ddot{a}$ are the wall velocity and acceleration, respectively.

Simulated bubbles were encapsulated by a shell modeled as a thin uniform viscoelastic solid (Hoff 2001) with a shear modulus G_s of 190 MPa, thickness d_s of 1.5 nm and a shear viscosity η_s of 0.07 Pa s. These parameters were based on the shell parameters for Definity estimated by Goertz *et al* (2007). The thickness of the shell was assumed to be constant and much smaller than the radius of the bubble. The model defines a nonlinear stress–strain relationship between the pressure difference across the shell and the radial expansion of the bubble. Thus, the influence of the shell is reduced as the bubble expands.

Unless otherwise stated, the simulations tested bubbles between 0.2 μm and 6 μm in diameter by exciting them with a 20 MHz, 30-cycle cos-tapered pulse with a peak-negative pressure of 1 MPa. To simulate the pressure dependence of the subharmonic, peak-negative pressures were varied between 100 kPa and 3 MPa.

2.2. Altering the bubble population

Definity (Bristol Myers Squibb, Boston, MA, USA) is a clinical contrast agent approved by the FDA for clinical echocardiography. The microbubbles comprise octofluoropropane (C_3F_8) gas encapsulated by a lipid shell. Though accurate size distributions are not available, mean diameters are in the range of 1.1 to 3.3 μm, with a large population of bubbles below 1 μm in diameter. 98% of the bubbles are below 10 μm in diameter (Bristol Myers Squibb 2002).

The native population of Definity was altered through a process of mechanical filtration to create three bubble populations varying in size distribution: the native population, a 5 μm filtered population and a 1.2 μm filtered population. The contrast agent was activated as instructed and mixed in a syringe with 30 mL of de-ionized and degassed water. This solution was then gently pushed through either a 1.2 μm or a 5 μm Acrodisc syringe filter (Pall Corp, New York, NY, USA) at an approximate rate of 6 ± 2 mL min^{-1}. These filters were the two largest pore sizes commercially available. The filter was replaced after 15 mL to reduce clogging of the filter pores. The filtrate was then further diluted with water to the desired concentration: 0.05% by volume for the native and 5 μm filtered populations, and 0.1% by volume for the 1.2 μm filtered population. Dilution ratios were based on the existing literature for similar experiments using Definity at high frequencies (Goertz 2002, Goertz *et al* 2005).

Size distributions were measured with a Coulter Multisizer III (Beckman Coulter Inc., Fullerton, CA, USA) using a 30 μm aperture, which resulted in a measurable size range of 0.6 to 18 μm. For each bubble population, concentrations were 0.05% by volume and measurements were repeated four times. The volume concentration was calculated from the number of bubbles per unit volume within each channel.

2.3. Backscatter experiments

Backscatter measurements were performed using a broadband 20 MHz focused PVDF transducer (20 mm focus, 7.5 mm aperture). The output pressures and beam characteristics of the transducer were determined with a 40 μm needle hydrophone (Precision Acoustics, UK) immersed in a water bath. **See endnote 1**

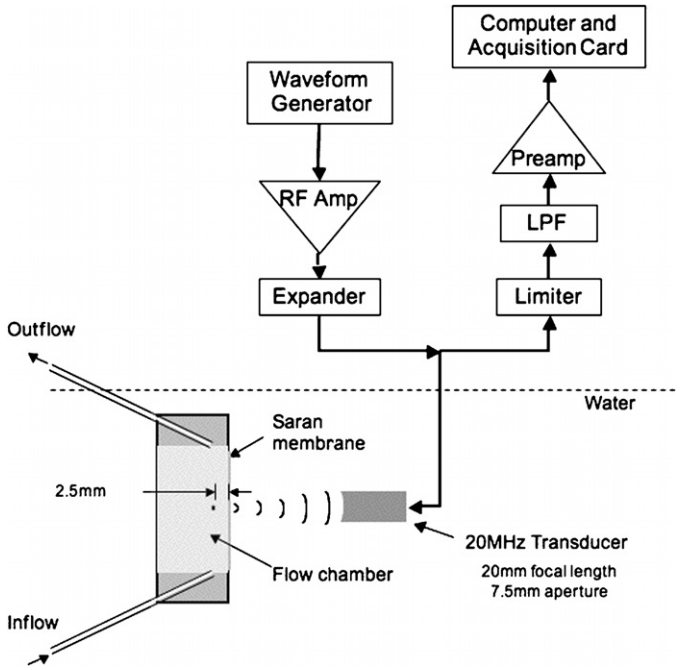

Figure 1. Experimental setup for backscatter experiments.

The transducer was focused inside a flow cell, 2.5 mm behind a window of Saran^{TM} wrap. The bubble population under test was circulated through the flow cell by gravity at a rate of 10 ± 4 mL min^{-1}, determined by measuring the volume of outflow over 1 min of flow. Excitation pulses were created with an arbitrary waveform generator (AWG2020, Tektronix, Beaverton, OR, USA), amplified by a 53 dB RF power amplifier (American Microwave Technology, Anaheim, CA) and passed through an expander to the transducer. Received signals were limited, low pass filtered at 70 MHz, amplified by a 40 dB pre-amplifier (AU-1313, Miteq Inc, Haupauge, NY, USA) and digitized at a sample rate of 500 MHz by an analog-to-digital card (DP240, Acqiris, Geneva, Switzerland) installed on a PC. A schematic representation of the experimental setup is illustrated in figure 1.

A 20 MHz, ten-cycle (9% -6 dB bandwidth) Gaussian-enveloped pulse with a peak-negative pressure of 380 kPa was used to determine the bubble size that contributes most to the subharmonic. Frequency dependence was tested using ten-cycle Gaussian enveloped pulses, varying in center frequency from 20 to 40 MHz. Peak-negative pressures varied between 380 kPa at 20 MHz and 1 MPa at 40 MHz such that subharmonic energy was visible above the noise floor. The pressure dependence of the subharmonic was observed by varying the peak-negative pressure of 20 MHz, ten-cycle Gaussian-enveloped pulses from 130 kPa to 1.3 MPa. To characterize the dependence on pulse bandwidth, 20 MHz, 380 kPa Gaussian-enveloped pulses were varied in duration between 2 cycles (50% -6 dB bandwidth) and 15 cycles (6% -6 dB bandwidth) at full-width half-maximum.

For each transmit condition, a series of 1000 pulses were transmitted at a pulse repetition frequency (PRF) of 50 Hz, ensuring a good representation of the population and enabling sufficient time for the flowing contrast agent to replenish the flow cell. A time window (3 μs Hamming window), corresponding to the depth of field of the transducer, was extracted from the received signal and analyzed. Spectra were averaged and corrected for electronic noise

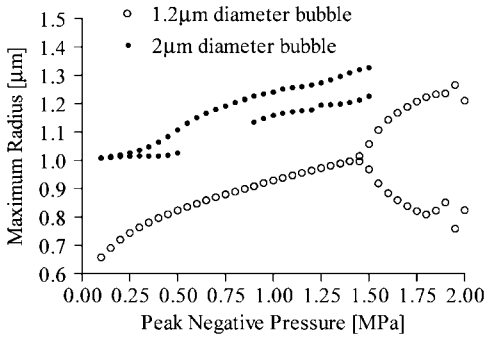

Figure 2. Maximum radius versus driving pressure for two shelled bubbles of different sizes. The radial oscillation of each bubble undergoes a bifurcation upon reaching a pressure threshold value. The subharmonic threshold is lower for the 2 μm bubble compared to the 1.2 μm bubble.

and the frequency response of the transducer as measured by quartz reflection. Each trial was repeated six times for each size distribution of bubbles. Error bars indicate a standard error between the six trials for all experiments, unless otherwise stated.

2.4. Coherence experiments

Coherent scattering from microbubbles is important for imaging regions of slow blood flow and implementing of Doppler and other multi-pulse techniques. To test signal coherence, the energy scattered from the microbubbles was observed for repeated insonation by either a low pressure (380 kPa) or a high pressure (3 MPa) ten-cycle 20 MHz Gaussian-enveloped pulse. The experimental backscatter apparatus described in figure 1 was used and, for each pulse tested, flow of the agent was stopped for 50 s to allow the bubbles to become relatively stationary. The excitation pulse was then transmitted 500 times at a PRF of 200 Hz. The flow was then resumed for 10 s to ensure that the flow cell was replenished with a fresh agent. The experiment was repeated 35 times for each pulse tested. Coherence was measured by selecting a region of interest containing a bubble signal and comparing it with subsequent pulses, observing signal decorrelation with respect to time. Both fundamental and subharmonic signals were extracted from the received signal by integrating the power spectra in a 2.5 MHz bandwidth surrounding the desired frequency.

3. Results

3.1. Numerical simulations

Numerical solutions of equation (1) were used to determine the resonance frequencies of free gas and encapsulated bubbles. As expected, the resonance frequencies varied inversely with the bubble diameter and increased with the inclusion of an encapsulating shell. The diameters of the shelled bubble ($G^s = 190$ MPa) resonant at 20 MHz and 10 MHz were predicted to be 1.2 μm (1.22) and 2 μm (1.96), respectively.

Numerical simulations of the Keller–Miksis model in equation (2) support the existence of a threshold for the generation of subharmonics. The 1.2 μm and 2 μm diameter bubbles described above were simulated at 20 MHz for a range of driving pressures. Figure 2 illustrates the local maxima of the bubbles' radii, plotted with respect to the driving pressure. For low amplitude pressures, the bubble's radius reached a single maximum, resulting in energy

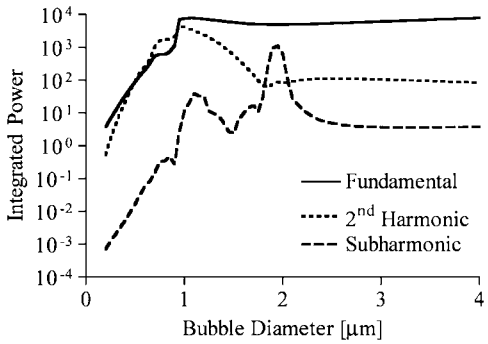

Figure 3. Scattered energy with respect to bubble size for a 1 MPa 20 MHz excitation. Large bubbles are responsible for the fundamental energy, 1 μm diameter bubbles are responsible for the second harmonic and 1.8 μm diameter bubbles are responsible for the subharmonic energy.

scattered at the fundamental frequency. Higher integer-ordered harmonics were also observed as the incident pressure was increased. Both the 1.2 μm diameter bubble excited at resonance and the 2 μm diameter bubble excited at its second harmonic undergo a bifurcation upon exceeding a threshold at 1.5 MPa and 250 kPa, respectively. For pressures greater than this threshold, the bubble's radius oscillated alternately between the two distinct maxima. This resulted in energy at half the driving frequency. As the pressure was increased further, the model predicted further bifurcations resulting in subharmonics at thirds and quarters of the driving frequency. The model also predicted regions of chaotic bubble oscillation as described by Lauterborn (1976).

The simulated bandwidth dependence of the subharmonic was investigated by observing the strength of the harmonic energy with respect to time. For the 1.2 μm diameter bubble, the subharmonic increased at a moderate rate, reaching a steady state maximum after ten cycles of radial oscillation. The 2 μm diameter bubble exhibited a large transient amount of subharmonic energy within the initial six cycles. The subharmonic signal then diminished before gradually redeveloping, requiring almost 30 cycles before reaching a steady state.

The contributions of each bubble size to the scattered harmonic energy of interest are presented in figure 3. 1 μm diameter bubbles contribute significantly to the fundamental signal. Bubbles larger than 1 μm diameter scatter increasing amounts of fundamental energy with an increasing geometric cross-section. The 1 μm diameter bubbles are also the primary contributors to the second harmonic. The subharmonic, however, arises primarily from bubbles 1.8 μm in diameter. At a first glance, this does not seem to support either hypothesis, since the bubbles resonant at 20 MHz and 10 MHz were determined to be 1.2 μm and 2 μm in diameter, respectively. This discrepancy, however, can be accounted for by considering the effect of increasing pressure amplitude on microbubble resonance frequency (MacDonald *et al* 2002). For low amplitude excitations, the resonance peak is as predicted by equation (1). For greater amplitudes, the resonance peak shifts toward the smaller bubbles.

3.2. Alteration of bubble population size distribution

Coulter counter size distribution measurements of the bubble populations are presented in figure 4. Despite the reduction in the total number of bubbles, the 5 μm and 1.2 μm filtered populations demonstrated an effective removal of the majority of bubbles larger than the filter pore size.

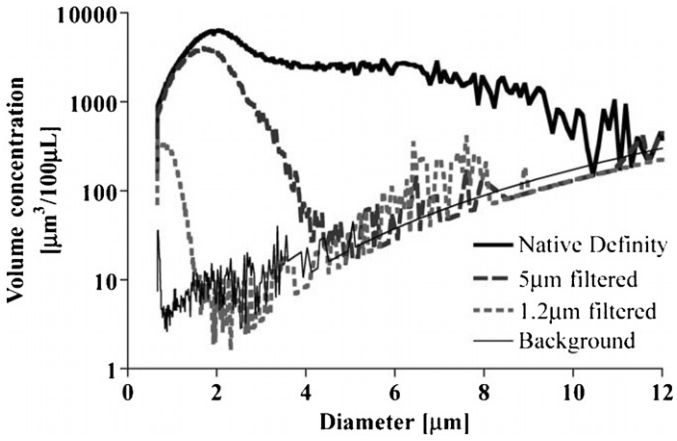

Figure 4. Coulter counter-size distribution measurements for native and altered Definity populations.

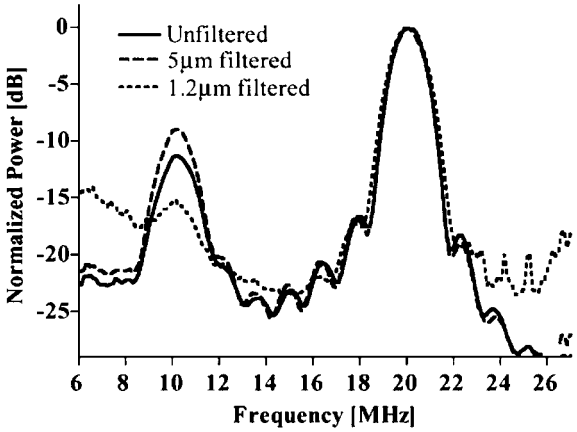

Figure 5. Power spectrum of different bubble populations excited at 20 MHz by a 380 kPa ten-cycle pulse. The power spectrum was normalized to the fundamental.

3.3. Backscatter experiments

Figure 5 illustrates the power spectrum of the backscattered signal from the three bubble populations normalized to the 20 MHz fundamental. Subharmonic energy at 10 MHz is observed for all three populations. The 5 μm filtered population resulted in the greatest amount of subharmonic energy, exhibiting a subharmonic -8.6 ± 0.3 dB below the fundamental. The native population and the 1.2 μm filtered population followed, producing subharmonic -10 ± 0.6 dB and -14.5 ± 0.2 dB below the fundamental, respectively.

As the driving frequency was varied from 20 MHz to 40 MHz, figure 6 illustrates the subharmonic-to-fundamental ratio for the three populations. At 20 MHz, the greatest subharmonic-to-fundamental ratio was produced by the 5 μm filtered population, followed by the native population and the 1.2 μm filtered population. As the driving frequency was increased past 32 MHz, however, the subharmonic-to-fundamental ratio of the 1.2 μm filtered population was observed to surpass that of the other two populations. For a driving frequency

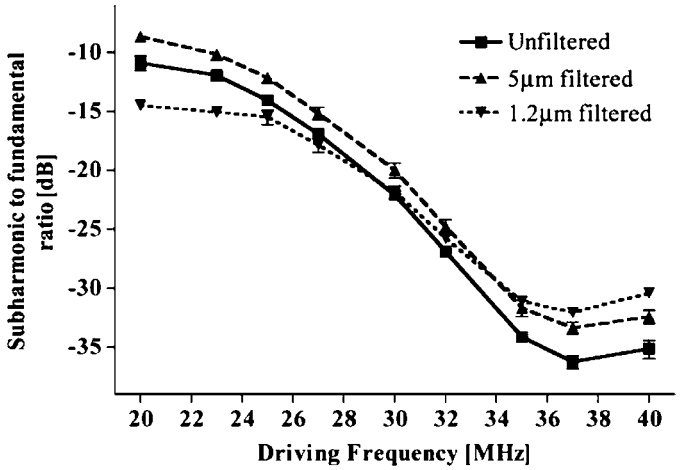

Figure 6. Ratio of the subharmonic to fundamental for the three bubble populations with respect to varying driving frequencies.

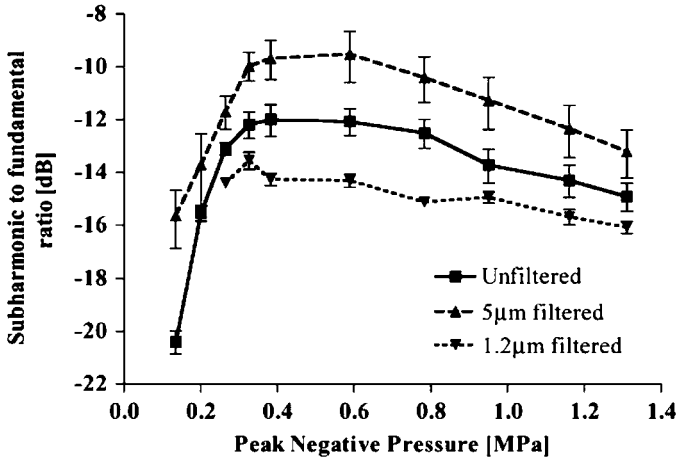

Figure 7. Ratio of the subharmonic to the fundamental for the three bubble populations is illustrated for varying driving pressures of a 20 MHz ten-cycle Gaussian pulse.

of 40 MHz, the subharmonic was -30.4 ± 0.3 dB, -32.4 ± 0.5 dB and -35.1 ± 0.8 dB below the fundamental for the 1.2 μm filtered, 5 μm filtered and native populations, respectively.

Experimentally measured subharmonic energy scattered from the three populations of bubbles is plotted with respect to pressure amplitude in figure 7. For pressures less than 320 kPa, the relative amount of subharmonic energy increased rapidly with incident pressure for both the 5 μm filtered and the native populations. The 5 μm filtered, native and 1.2 μm filtered populations exhibited a maximum subharmonic-to-fundamental ratio of -9.5 ± 1 dB, -12.0 ± 0.6 dB and -13.6 ± 0.3 dB, respectively, for pressures between 380 kPa and 590 kPa. For pressures greater than 320 kPa, the absolute power of the subharmonic begins to saturate, resulting in an observed decrease in the subharmonic-to-fundamental ratio since the fundamental energy continues to increase with pressure. A subharmonic signal was

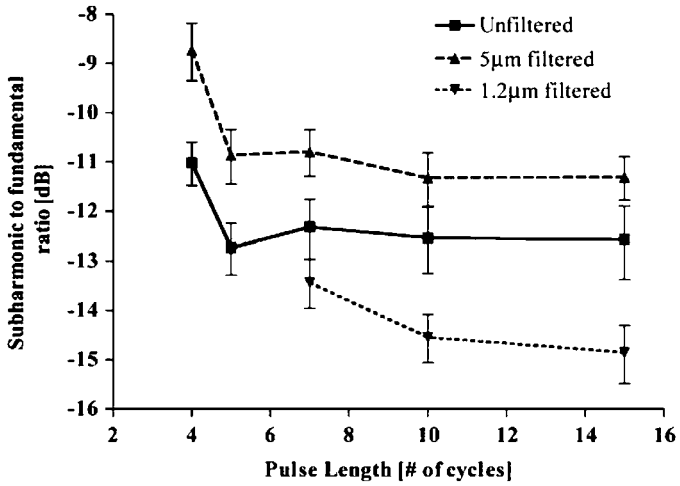

Figure 8. Ratio of the subharmonic to the fundamental for the three bubble populations is illustrated for 20 MHz 380 kPa Gaussian pulses of varying bandwidths.

not discernable from the noise floor for pressures below 130 kPa for the native and 5 μm filtered populations and 260 kPa for the 1.2 μm filtered population. For pressures greater than 260 kPa, the 1.2 μm filtered population exhibits a subharmonic signal constant with increasing pressure amplitude. The fundamental signal, however, continues to increase resulting in an observed decrease in the subharmonic-to-fundamental ratio.

The effect of varying the bandwidth of the excitation pulse is illustrated in figure 8. The subharmonic was not discernable for wide bandwidth pulses less than four cycles in duration. This was due in part to the bandwidth of the adjacent fundamental signal and the height of the side lobes and noise floor. The 5 μm filtered population and the native population exhibited a maximum subharmonic signal relative to the fundamental for pulse bandwidths four cycles in duration. The subharmonic was observed -8.7 ± 0.6 dB and -11.0 ± 0.4 dB below the fundamental. The 1.2 μm filtered population exhibited a maximum subharmonic -13.4 ± 0.5 dB below the fundamental for seven-cycle pulses, the most wideband pulse tested that produced a distinct subharmonic signal. As the pulse bandwidth was decreased, the noise floor was reduced significantly due to the increased scattered power at the fundamental and harmonic frequencies. While the absolute strength of the subharmonic and the fundamental increased logarithmically, the amount of the subharmonic relative to the level of the fundamental decreased with increasingly narrowband pulses for all three populations. The subharmonic signal from the 1.2 μm filtered population was not visible for pulses less than seven cycles in duration.

3.4. Coherence

The decorrelation of the fundamental and subharmonic signals with respect to repeated insonation is presented in figure 9. The fundamental signal from the bubbles excited by the 3 MPa pulse decorrelates over a period of 200 ms, while the 380 kPa pulse requires almost 700 ms to decorrelate. More noise was associated with the coherence of the signal since the absolute strength of the subharmonic signal was significantly less. Excited by the 380 kPa pulse, however, the subharmonic signal remains coherent for more than 400 ms. The 3 MPa pulse resulted in decorrelation at a much greater rate.

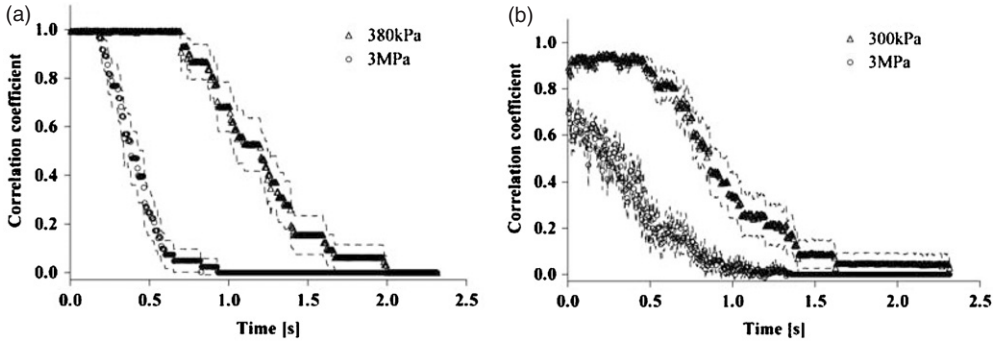

Figure 9. Decorrelation of the fundamental (a) and subharmonic (b) signals after repeated exposure to 20 MHz ten-cycle Gaussian pulses at 380 kPa and 3 MPa. PRF = 200 Hz. Dashed lines surrounding indicate a standard error.

4. Discussion

Subharmonic imaging techniques offer the potential for near-complete tissue suppression due to the uniqueness of the subharmonic energy produced by microbubbles. While the use of half the operating frequency results in an inherent loss in resolution, preliminary *in vivo* experiments have demonstrated the feasibility of subharmonic imaging at an operating frequency of 20 MHz to detect blood flow in the microcirculation (Goertz *et al* 2005). The goals of this research were to determine the origin of this subharmonic energy from clinical contrast agents and to determine the optimal transmit conditions for subharmonic imaging at high frequencies.

It was hypothesized that larger bubbles, excited at their second harmonic, would produce the majority of the coherent subharmonic signal observed from clinical contrast agents at high frequencies. This hypothesis was supported by numerical solutions of the Keller–Miksis model. For example, figure 2 shows that the threshold for subharmonic production is lower for a 2 μm diameter bubble than for a 1.2 μm diameter bubble. Figure 3 demonstrated that shelled bubbles 1.8 μm in diameter scattered significantly more energy at half the driving frequency than any other sized bubble in the population. These bubbles were determined to be resonant at 10 MHz and, consequently, were excited at their second harmonic.

Experiments that altered the size distribution of the population demonstrated that for the 20 MHz driving frequency, the 5 μm filtered population produced the greatest amount of subharmonic energy relative to the fundamental. Since the bubbles of the 1.2 μm filtered population are completely contained within the 5 μm filtered population, it can be concluded that the bubbles of Definity between 1.2 μm and 5 μm are responsible for much of the subharmonic signal. It was demonstrated previously that Definity bubbles less than 2 μm in diameter and bubbles less than 1 μm in diameter produced significant attenuation above 15–20 MHz and 40 MHz, respectively (Goertz *et al* 2007).

Numerical simulations predicted that the resonant diameter of a bubble would vary inversely with the driving frequency. Consequently, if the observed subharmonic was caused by either bubbles excited at their resonant frequency or bubbles excited at their second harmonic, then the size of the responsible bubble should decrease with increasing driving frequency. This hypothesis was supported by experimental results illustrated in figure 6. For a 20 MHz driving frequency, it was determined that bubbles between 1.2 μm and 5 μm diameter were primarily responsible for the observed subharmonic. As the driving frequency

exceeds 32 MHz, however, the level of the subharmonic relative to the fundamental from the 1.2 μm filtered population surpassed that of both the 5 μm filtered population and the native population. This suggests that bubbles of Definity smaller than 1.2 μm diameter are primarily responsible for the observed subharmonic for driving frequencies greater than 32 MHz. It also suggests that larger bubbles, not present in the 1.2 μm filtered population, contribute energy only to the fundamental and higher integer-ordered harmonics, thus decreasing the ratio of the subharmonic to the fundamental.

In order to differentiate between bubbles excited at resonance and bubbles excited at their second harmonic, the incident pressure was varied. Numerical simulations predicted not only the existence of a subharmonic threshold, but also that this threshold was at a minimum for bubbles excited at their second harmonic. The model also suggested that bubbles of any size could be driven to generate subharmonic energy if the bubble-specific pressure threshold was exceeded. Experiments, illustrated in figure 7, varied the incident pressure amplitude of 20 MHz driving pulses and supported the existence of a subharmonic threshold. For both the native population and the 5 μm filtered population, regions of subharmonic growth and saturation were observed. These regions were described for Levovist (Schering AG, Berlin) excited at 2 MHz (Shi *et al* 1999) and an experimental lipid encapsulated agent at 30 MHz (Goertz *et al* 2006a). In the region of subharmonic growth, the levels of the subharmonic were observed to increase by 6–8 dB over the pressure range of 130 kPa to 320 kPa. As the pressure was increased further, the strength of the subharmonic was observed to saturate and then decrease relative to the fundamental. This decrease was determined to result from increased amounts of energy scattered at the fundamental; absolute levels of the subharmonic remained constant. No region of growth was observed for the 1.2 μm filtered population. These pressure thresholds were slightly less than those observed by Goertz *et al* (2007) (saturation observed at 500 kPa) though still comparable given the higher center frequency used in their experiments.

Numerical simulations that demonstrated the bandwidth dependence of the subharmonic suggested that stable subharmonic oscillations from resonant bubbles developed over a period of ten cycles before saturating. Larger bubbles, excited at their second harmonic, immediately began oscillating at their resonant frequency. Whether this response was a function of the properties of the bubble or the transmission of energy through sidebands of the driving pulse or both remains unclear. Experiments illustrated in figure 8 varied the pulse length between 2 and 15 cycles (-6 dB bandwidth of 50 to 6%), but did not enable differentiation between the two hypothesized origins of the subharmonic signal. The fundamental increased at a faster rate than the absolute subharmonic signal causing the decrease in the subharmonic signal relative to the fundamental. The 5 μm filtered population continued to result in the highest subharmonic-to-fundamental ratio, while the native population and the 1.2 μm filtered population followed, respectively.

Experiments illustrated in figure 9 demonstrated that the 380 kPa 20 MHz ten-cycle Gaussian pulse used in previous experiments did not result in the rapid decorrelation of signal associated with bubble disruption. Even after repeated insonation at 200 Hz, the signals remained coherent for more than 600 ms. This exceeds the length of time predicted for the diffusion of gas into a liquid and the reported duration of bubble disruption (Klibanov 2002). Further, 380 kPa is well under the 1.8 MPa pressure threshold that was observed to create broadband acoustic emissions at 30 MHz (Goertz *et al* 2006a). It is suspected, consequently, that the observed signal decorrelation is due to the motion of the bubbles from the focus of the ultrasound beam. This motion may arise from floatation, Brownian motion or radiation forces caused by the incident pulses. The coherence of the subharmonic signal was also observed specifically.

The Keller–Miksis model suffers from a number of limitations and consequently was only used to guide experimental design. While radial expansions did not exceed twice the equilibrium radius (Vokurka 1986), the model was developed and intended for clinical frequencies and low amplitude excitations. The consideration of only spherical modes of oscillation may not be appropriate as the wavelength of the incident ultrasound approaches the size of the bubble. The shell model, furthermore, was fitted using parameters determined from experimental observations of Definity microbubbles (Goertz *et al* 2007). Similar values have been reported for other lipid encapsulated agents (Gorce *et al* 2000, Hoff *et al* 2000, Sarkar *et al* 2005).

Coulter counter-measurements presented in figure 4 demonstrate the effectiveness of the filtration technique. With the 5 μm filter, bubbles larger than 5 μm were successfully removed. Measurements of the 1.2 μm filtered population suggested that a few bubbles larger than the filter pore size might have escaped filtration. The filtration process also significantly decreased the volume fraction of the bubbles in the 1.2 μm filtered population. To increase the signal-to-noise ratio, the concentration of the 1.2 μm filtered population was increased to 0.1% by volume before filtration. It is unknown if any of the bubble properties were altered during the process. Filtration and decantation have been demonstrated to be effective techniques to alter the bubble population of Definity. Gravity filtration using a large surface area membrane effectively removed bubbles larger than 1 μm in diameter (Goertz *et al* 2007). This may be a more effective technique for future experiments.

Subharmonic imaging techniques can be improved by maximizing the subharmonic energy produced by contrast agents. These experiments demonstrate that this can be accomplished by manufacturing contrast agents of specific size distributions that correspond to the intended driving frequency: for applications operating between 20 and 32 MHz, size distributions of Definity should be between 1.2 μm and 5 μm in diameter, and for frequencies between 32 and 40 MHz, contrast agents should be less than 1.2 μm in diameter.

The optimal transmit conditions for generating subharmonic signal from Definity microbubbles in water have also been described. For 20 MHz driving frequencies, pressure amplitudes between 380 kPa and 590 kPa and pulses four-cycles in duration produced the greatest amount of subharmonic energy relative to the fundamental. Subharmonic imaging implemented with band-pass filtering (Goertz *et al* 2005) or pulse inversion (Goertz *et al* 2006b), however, requires a high subharmonic signal relative to the surrounding tissue, not the fundamental. Narrowband pulses maximize the amount of subharmonic generated relative to the tissue and reduce overlap of the subharmonic by the adjacent fundamental signal. The loss of axial resolution, however, should be considered.

5. Conclusion

The behavior of the observed subharmonic signal from bubbles of Definity in water was described for variations in bubble size distribution, driving frequency, pressure amplitude and pulse bandwidth. For frequencies in the 20–32 MHz range, bubbles between 1.2 μm and 5 μm diameter were responsible for the majority of the subharmonic. For frequencies between 32 MHz and 40 MHz, the majority of the subharmonic originates from bubbles less than 1.2 μm in diameter. For a driving frequency of 20 MHz, a four-cycle pulse with peak-negative pressure between 380 kPa and 590 kPa generated the maximal amount of subharmonic relative to the fundamental. The coherence of the subharmonic signal also supports the feasibility of implementing Doppler and multi-pulse techniques for subharmonic imaging.

Acknowledgments

The authors acknowledge the financial support of the Canadian Institutes of Health Research, the National Cancer Institute of Canada/Terry Fox Foundation, the Ontario Research and Development Challenge Fund and Visualsonics Inc. FSF wishes to disclose a financial relationship with Visualsonics.

References

Becher H and Burns P N 2000 *Handbook of Contrast Echocardiography* (Berlin: Springer)

Bristol Myers Squibb 2002 *Definity* www.definityimaging.com, accessed 19 December 2003

Burns P N 1996 Harmonic imaging with ultrasound contrast agents *Clin. Radiol.* **51 (Suppl 1)** 50–5

Chang P H, Shung K K, Wu S and Levene H B 1995 Second harmonic imaging and harmonic Doppler measurements with Albunex *IEEE Trans. Ultrason. Ferroelectr. Freq. Control* **42** 1020–6

Chomas J, Dayton P, May D and Ferrara K 2002 Nondestructive subharmonic imaging *IEEE Trans. Ultrason. Ferroelectr. Freq. Control* **47** 883–92

Dayton P A and Ferrara K W 2002 Targeted imaging using ultrasound *J. Magn. Reson. Imaging* **16** 362–77

de Jong N, Bouakaz A and Frinking P 2002 Basic acoustic properties of microbubbles *Echocardiography* **19** 229–40

Eller A and Flynn H 1969 Generation of subharmonics of order one-half by bubbles in a sound field *J. Acoust. Soc. Am.* **46** 722–7

Forsberg F, Shi W T and Goldberg B B 2000 Subharmonic imaging of contrast agents *Ultrasonics* **38** 93–8

Foster F S, Burns P N, Simpson D H, Wilson S R, Christopher D A and Goertz D E 2000a Ultrasound for the visualization and quantification of tumor microcirculation *Cancer Metastasis Rev.* **19** 131–8

Foster F S, Pavlin C J, Harasiewicz K A, Christopher D A and Turnbull D H 2000b Advances in ultrasound biomicroscopy *Ultrasound Med. Biol.* **26** 1–27

Goertz D E 2002 *Imaging the Microcirculation with High Frequency Ultrasound* (Toronto: University of Toronto)

Goertz D E, Cherin E, Needles A, Karshafian R, Brown A S, Burns P N and Foster F S 2005 High frequency nonlinear B-scan imaging of microbubble contrast agents *IEEE Trans. Ultrason. Ferroelectr. Freq. Control* **52** 65–79

Goertz D E, de Jong N and van der Steen A F 2007 Attenuation and size distribution measurements of definity (TM) and manipulated definity (TM) populations *Ultrasound. Med. Biol.* at press **See endnote 2**

Goertz D E, Frijlink M, Bouakaz A, Chin C T, de Jong N and van der Steen A 2003 The effect of bubble size on nonlinear scattering from microbubbles *IEEE Ultrasonics Symp. (Hawaii, USA)* pp 1503–6

Goertz D E, Frijlink M, de Jong N and van der Steen A 2004 High frequency nonlinear scattering and imaging of a submicron contrast agent *IEEE UFFC (Montreal, Canada)* pp 986–9

Goertz D E, Frijlink M E, de Jong N and van der Steen A F 2006a High frequency nonlinear scattering from a micrometer to submicrometer sized lipid encapsulated contrast agent *Ultrasound Med. Biol.* **32** 569–77

Goertz D E, Frijlink M E, de Jong N and van der Steen A F 2006b Nonlinear intravascular ultrasound contrast imaging *Ultrasound Med. Biol.* **32** 491–502

Gorce J M, Arditi M and Schneider M 2000 Influence of bubble size distribution on the echogenicity of ultrasound contrast agents: a study of SonoVue *Invest. Radiol.* **35** 661–71

Hoff L 2001 *Acoustic Characterization of Contrast Agents for Medical Ultrasound Imaging* (Dordrecht: Kluwer)

Hoff L, Sontum P C and Hovem J M 2000 Oscillations of polymeric microbubbles: effect of the encapsulating shell *J. Acoust. Soc. Am.* **107** 2272–80

Kerbel R S 2001 Clinical trials of antiangiogenic drugs: opportunities, problems, and assessment of initial results *J. Clin. Oncol.* **19** 45S–51S

Klibanov A 2002 Ultrasound contrast agents: development of the field and current status *Top. Curr. Chem.* **222** 73–105

Krishna P D, Shankar P M and Newhouse V L 1999 Subharmonic generation from ultrasonic contrast agents *Phys. Med. Biol.* **44** 681–94

Lauterborn W 1976 Numerical investigations of nonlinear oscillations of gas bubbles in liquids *J. Acoust. Soc. Am.* **59** 283–93

Leighton T 1994 *The Acoustic Bubble* (London: Academic)

Lockwood G R, Ryan L K, Hunt J W and Foster F S 1991 Measurement of the ultrasonic properties of vascular tissues and blood from 35–65 MHz *Ultrasound Med. Biol.* **17** 653–66

MacDonald C, Sboros V, Retkute R, Gomatam J, Pye S D, Moran C M and McDicken W N 2002 A numerical investigation into the effects of increasing pressure amplitude on microbubble resonance frequency *IEEE UFFC Symp. (Munich)* pp 1937–40

Neppiras E 1980 Acoustic cavitation *Phys. Rep.* **61** 159–251

Phelps A D and Leighton T G 1997 The subharmonic oscillations and combination-frequency subharmonic emissions from a resonant bubble: their properties and generation mechanisms *Acustica* **83** 59–66

Plesset M and Prosperetti A 1977 Bubble dynamics and cavitation *Annu. Rev. Fluid Mech.* **9** 145–85

Sarkar K, Shi W T, Chatterjee D and Forsberg F 2005 Characterization of ultrasound contrast microbubbles using in vitro experiments and viscous and viscoelastic interface models for encapsulation *J. Acoust. Soc. Am.* **107** 539–50

Shankar P M, Krishna P D and Newhouse V L 1999 Subharmonic backscattering from ultrasound contrast agents *J. Acoust. Soc. Am.* **106** 2104–10

Shi W T, Forsberg F and Goldberg B B 1997 Subharmonic imaging with gas-filled microbubbles *J. Acoust. Soc. Am.* **101** 3139

Shi W T, Forsberg F, Raichlen J, Needleman L and Goldberg B B 1999 Pressure dependence of subharmonic signals from contrast microbubbles *Ultrasound Med. Bio.* **25** 275–83

Shi W T, Hoff L and Forsberg F 2002 Subharmonic performance of contrast microbubbles: an experimental and numerical investigation *IEEE UFFC Proc* pp 1957–60

Shung K K and Thieme G 1993 *Ultrasonic Scattering in Biological Tissues* (Boca Raton, FL: CRC Press)

Simpson D H, Chin C T and Burns P N 1999 Pulse inversion doppler: a new method for detecting nonlinear echoes from microbubble contrast agents *IEEE Trans. Ultrason. Ferroelectr. Freq. Control* **46** 372–81

Vokurka K 1986 Comparison of Rayleigh's, Herring's, and Gilmore's models of gas bubbles *Acustica* **59** 214–9

Endnotes

(1) Author: Please provide the expanded form of 'PVDF'.
(2) Author: Please update reference 'Goertz *et al* 2007'.
